Chinese Journal of
POLYMER SCIENCE

RESEARCH ARTICLE

https://doi.org/10.1007/s10118-025-3365-z
Chinese J. Polym. Sci. **2025**, *43*, 1333–1345

Sustainable Flame-retardant and Tough Poly(vinyl alcohol) Films with Phytic Acid and Biochar: A Simple and Effective Approach

Chang-Fa Zhu[a,†], Jia-Xi Zhang[a,†], Shao-Ping Qian[a,b*], and Tong-Hui Pan[a]

[a] *School of Materials Science and Chemical Engineering, Ningbo University, Ningbo 315211, China*
[b] *Key Laboratory of Impact and Safety Engineering, Ministry of Education, Ningbo University, Ningbo 315211, China*

Electronic Supplementary Information

Abstract Poly(vinyl alcohol) (PVA) is a biodegradable and environmentally friendly material known for its gas barrier characteristics and solvent resistance. However, its flammability and water sensitivity limit its application in specialized fields. In this study, phytic acid (PA) was introduced as a halogen-free flame retardant and biochar (BC) was introduced as a reinforcement to achieve both flame resistance and mechanical robustness. We thoroughly investigated the effects of BC particle sizes (100–3000 mesh) and addition amounts (0 wt%–10 wt%), as well as PA addition amounts (0 wt%–15 wt%), on the properties of PVA composite films. Notably, the PA10/1000BC5 composite containing 10 wt% PA and 5 wt% 1000 mesh BC exhibited optimal properties. The limiting oxygen index increased to 39.2%, and the UL-94 test achieved a V-0 rating. Additionally, the PA10/1000BC5 composite film demonstrated significantly enhanced water resistance, with a swelling ratio reaching 800% without dissolving, unlike that of the control PVA. The water contact angle was 70°, indicating that hydrophilic properties remained essentially unaffected. Most importantly, the tensile modulus and elongation at break were 213 MPa and 281.7%, respectively, nearly double those of the PVA/PA composite film. This study presents an efficient and straightforward method for preparing PVA composite films that are flame-retardant, tough, and water-resistant, expanding their potential applications in various fields.

Keywords Poly(vinyl alcohol); Phytic acid; Biochar; Flame retardancy; Fracture toughness

Citation: Zhu, C. F.; Zhang, J. X.; Qian, S. P.; Pan, T. H. Sustainable flame-retardant and tough poly(vinyl alcohol) films with phytic acid and biochar: a simple and effective approach. *Chinese J. Polym. Sci*. **2025**, *43*, 1333–1345.

INTRODUCTION

With the acceleration of industrialization, plastics have become ubiquitous in various sectors, owing to their ease of processing, cost-effectiveness, chemical stability, and corrosion resistance.[1] Poly(vinyl alcohol) (PVA) is a biodegradable polymer known for its eco-friendliness, gas-barrier characteristics, and solvent resistance, making it highly useful in composite films and packaging.[2] However, like most polymer materials, PVA is highly flammable owing to its composition and chemical structure. This flammability not only leads to rapid decomposition or combustion but also produces significant quantities of toxic volatile compounds and dripping molten liquids, potentially triggering secondary fires.[3–7] Consequently, the use of PVA in critical sectors such as construction, transportation, and electrical and electronic equipment is restricted.[8] This fact has spurred significant research on the flame-retardant modification of PVA.

The primary methods for flame-retardant modification of PVA include the addition of flame retardants and the incorporation of flame-retardant groups or elements into the material structure. The former is preferred because of its simplicity and effectiveness.[9,10] However, traditional halogen flame retardants produce large amounts of smoke and release hydrogen halide gases during combustion, causing serious environmental pollution and health threats.[11,12] In response, halogen-free flame retardants such as phytic acid (PA), chitosan, and tannic acid have gained attention.[13–16] PA is increasingly being used in the synthesis of new flame retardants owing to its biocompatibility and degradability. However, the synthetic process often involves chemical reagents, which can be cumbersome and may result in some degree of pollution, limiting its suitability for practical applications. In contrast, the six phosphate groups in PA make it an excellent flame retardant. Direct utilization of PA can simplify the preparation process and reduce the use of chemical reagents, while also reducing costs.

Despite these advances, the limited ductility of PVA makes it prone to cracking during processing, and its relatively low elongation rate poses a challenge in film production. Additionally, the high hydroxyl content of PVA contributes to its water sensitivity, resulting in swelling and dissolution in water, limiting its suitability for use in moist environments.[17] Previous research has shown that adding reinforcing fillers,

* Corresponding author, E-mail: qianshaoping@nbu.edu.cn
† These authors contributed equally to this work.
Received January 27, 2025; Accepted April 23, 2025; Published online July 8, 2025

such as graphene oxide, montmorillonite, carbon nanotubes, biochar, and cellulose[18–22] can significantly improve the mechanical strength, thermal stability, and moisture resistance of PVA. Among these materials, biochar (BC) is particularly notable for its porous structure, large surface area, and low density. Mozrall *et al.*[23] reported that different amounts and particle sizes of BC exhibited varying degrees of enhancement in the strength and toughness of composite materials. Barbalini *et al.*[24] reported that immersing cotton fabrics in a mixed aqueous solution of BC and PA significantly enhanced flame retardancy. Under limited oxygen conditions, the treated fabric underwent thermal chemical conversion to form a carbon-rich protective layer. However, the flame-retardant effect diminished after washing, suggesting that PA and BC were physically adsorbed onto the cotton fabric rather than forming durable bonds. In contrast, PA and BC establish a stable chemical network with PVA through hydrogen bonding, ensuring persistent flame-retardant properties. The particle size of BC plays a crucial role in its dispersion within the composite material, which influences the overall performance of the composite. Therefore, investigating the effects of BC particle size is essential for optimizing the material properties and improving the performance of PVA composite films.

This study aimed to explore a method for modifying PVA by combining halogen-free flame retardants (PA) with reinforcing fillers (BC) to enhance its flame retardancy and mitigate the decline in mechanical properties. This study presents the first report on the preparation of PVA composite films with flame retardant and high toughness properties using PA and BC. By elucidating the synergistic effects of PA and BC on mechanical reinforcement and flame retardancy, this work significantly enhances the mechanical properties, flame resistance, and water durability of films, offering valuable insights for the rational design of multifunctional composite materials with broad application potential. We examined the effects of different concentrations of PA, BC particle sizes, and levels of addition on the flame retardancy, mechanical properties, thermal stability, and water sensitivity of PVA to determine the optimal modification formulation. This research is poised to create a novel flame-retardant composite material system, offering new perspectives and methods for the flame-retardant modification of PVA polymers with significant research implications.

EXPERIMENTAL

Materials

Poly(vinyl alcohol) (PVA, 1799), with a polymerization degree of 1700 and an alcoholysis degree of 99%, was purchased from Hongshang Chemical Technology Co., Ltd. (Shanghai, China). Phytic acid aqueous solution (70 wt%) was purchased from Maclin Biochemical Co., Ltd. (Shanghai, China). Biochar (100M, 1000M, 2000M, 3000M) was supplied by Wanglin Biotechnology Co. Ltd. (Zhejiang, China). The biochar was derived from bamboo (*Phyllostachys edulis*) particles, which were pyrolyzed in an oxygen-deficient environment at 500 °C for 4 h in a mechanical kiln, followed by washing with water and drying. All other reagents were obtained from conventional commercial sources without further purification.

Preparation of PVA/PA/BC Composite Films

Fig. 1 shows the preparation process of the PVA/PA/BC composite film. Specifically, PVA (5.4 g) was initially dissolved thoroughly in 30 mL of deionized water, and then different amounts of the PA/BC mixed solution were added. Henceforth, the film-forming blends were then homogenized using a magnetic stirrer for 2 h at 95 °C. The resulting suspensions of PVA/PA/BC were cast into circular Petri dishes, allowed to air-dry for 30 min at room temperature, and dried in an oven for 20 h at 65 °C to obtain the PVA/PA/BC composite films.

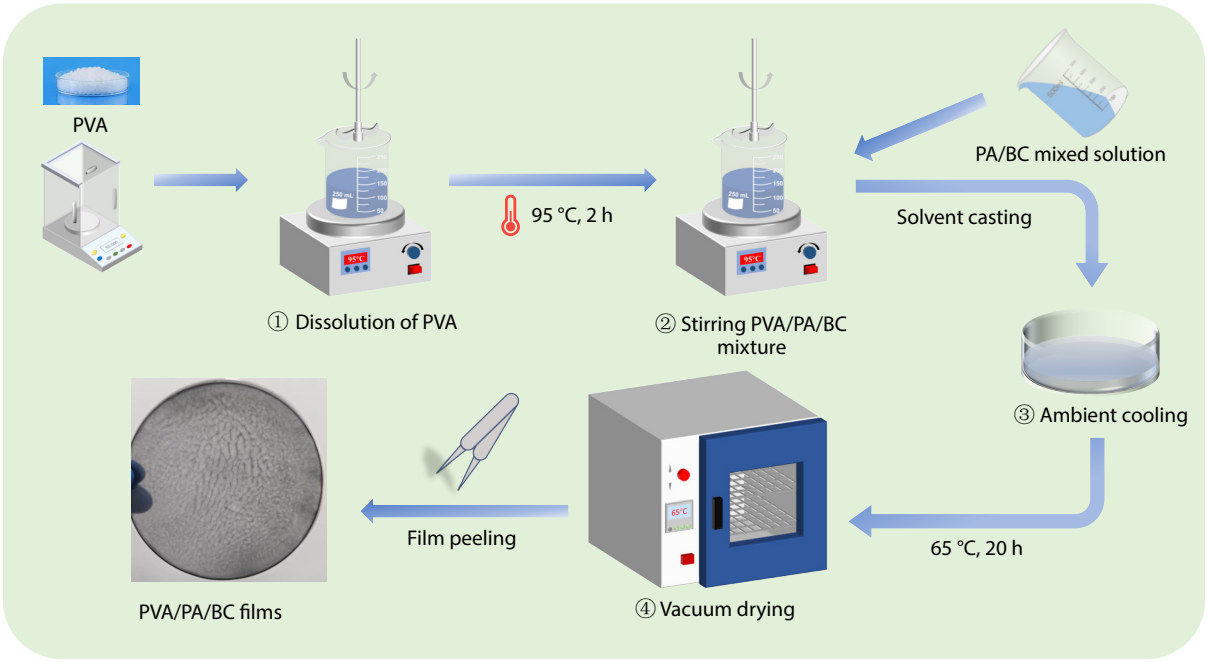

Fig. 1 Schematic diagram of the preparation process of PVA/PA/BC composite films.

https://doi.org/10.1007/s10118-025-3365-z

The compositions and abbreviations of the composite films are shown in Table 1. The analysis of the impact of BC particle size was based on samples PA10/100BC5, PA10/1000BC5, PA10/2000BC5, and PA10/3000BC5. The analysis of the impact of PA addition was based on samples PA5/1000BC5, PA10/1000BC5, and PA15/1000BC5. The analysis of the impact of BC addition was based on samples PA10/1000BC2, PA10/1000BC5, PA10/1000BC8, and PA10/1000BC10. PVA, PVA/BC and PVA/PA were used as references for basic performance.

Fourier Transform Infrared Spectroscopy (FTIR)

The FTIR analysis of the composite films was performed using a Nicolet 6700 spectrometer (Thermo Fisher, USA). The spectra were obtained over a wavenumber range of 4000–500 cm^{-1}, utilizing the KBr pellet method.[25] Each spectrum was collected over 64 scans with a resolution of 1 cm^{-1}.

Mechanical Tests

The mechanical properties were evaluated by subjecting the composite films to tensile tests at room temperature using a universal testing machine (CMT4503, MTS, Inc., Jinan, China). The tensile testing adhered to ASTM D638 standards with a crosshead speed of 20 mm/min and a gauge length of 20 mm. Each sample was cut into dumbbell-shaped specimens measuring 50 mm × 4 mm × 0.2 mm. To ensure reliable results, five specimens from each composite-film group were tested.[26]

Scanning Electron Microscope (SEM) and Energy-dispersive X-ray Spectroscopy (EDS) Analysis

SEM analysis was used to examine the fracture surfaces after tensile testing and the cross-sections after combustion. The Hitachi S-8010 SEM (Japan) was operated at an acceleration voltage of 5 kV. Prior to imaging, a thin layer of gold was sputter-coated onto the film surfaces to enhance conductivity. EDS was performed using an electron beam with an energy of 10 kV to analyze the elemental composition. The analysis was conducted with a working distance of 7 mm using an energy spectrometer (Oxford Instruments X-Max^N) attached to the SEM.

Thermogravimetric Analysis (TGA)

TGA was conducted using an STA 2500 analyzer (Netzsch, Germany) under nitrogen gas. Samples weighing 5.0–7.0 mg were placed in a standard alumina crucible, with an empty crucible as a reference. The samples were heated from 30 °C to 600 °C at a rate of 10 °C/min with a nitrogen flow rate of 50 mL/min.

Combustion Behavior

The combustion performance was evaluated using a vertical burning test, limiting oxygen index (LOI), and cone calorimetry test (CCT). The LOI was measured using an oxygen index tester (BJY-JF-3, Zhejiang, China) according to the GB/T2406 standards. The samples for this test were 150 mm × 50 mm × 0.2 mm. Vertical burning tests followed the ISO 9773 guidelines, using a vertical flame tester (ZRS-TC, Jiangsu, China), with samples sized 150 mm × 50 mm × 0.2 mm. The CCT was performed using a cone calorimeter tester (Vouch6810, Hunan, China) under a heat flux of 50 kW/m^2, and the samples measuring 100 mm × 100 mm × 0.3 mm were tested according to the ISO 5660-1 standard.

Swelling Properties

The swelling properties of the PVA composite films were evaluated by submerging the film samples, each cut to dimensions of 20 mm × 10 mm, in deionized water at 20 °C for 1 h. After immersion, excess water was gently blotted away using filter paper.[27] The initial mass (M_0) and mass after swelling (M_t) were measured, and the swelling ratio (SWR) was computed based on Eq. (1).

$$\mathrm{SWR}\ (\%) = \frac{M_t - M_0}{M_0} \times 100\% \quad (1)$$

Wettability Analysis

The surface wettability of the samples was evaluated using an Easy-Drop Standard goniometer (DSA 100, Krüss GmbH, Hamburg, Germany) with specialized software employed to capture images and analyze data. Each drop of distilled water had a volume of 5 μL, and measurements were taken from at least five separate samples, which were then averaged.

Statistical Analysis Methods

The data presented represent the average values from five individual measurements. A one-way analysis of variance (ANOVA) was employed to analyze differences between the groups, with statistical significance considered at $p < 0.05$.[28]

RESULTS AND DISCUSSION

Characterization of BC

The surface functional groups of BC are shown in Fig. 2(a). Char-

Table 1 Sample compositions.

Sample	Mesh Size of BC	Component		
		PVA (wt%)	PA (wt%)	BC (wt%)
PVA	–	100	–	–
PVA/BC	1000	100	–	5
PVA/PA	–	100	10	–
PA10/100BC5	100	100	10	5
PA10/1000BC2	1000	100	10	2
PA10/1000BC5	1000	100	10	5
PA10/1000BC8	1000	100	10	8
PA10/1000BC10	1000	100	10	10
PA5/1000BC5	1000	100	5	5
PA15/1000BC5	1000	100	15	5
PA10/2000BC5	2000	100	10	5
PA10/3000BC5	3000	100	10	5

Note: The amounts of PA and BC are based on the weight of PVA. The name of PVA/PA/BC composite film is set as PA*x*/y*y*BC*z*, where *x* represents the amount of PA added, *y* represents the mesh size of BC, and *z* represents the amount of BC added.

https://doi.org/10.1007/s10118-025-3365-z

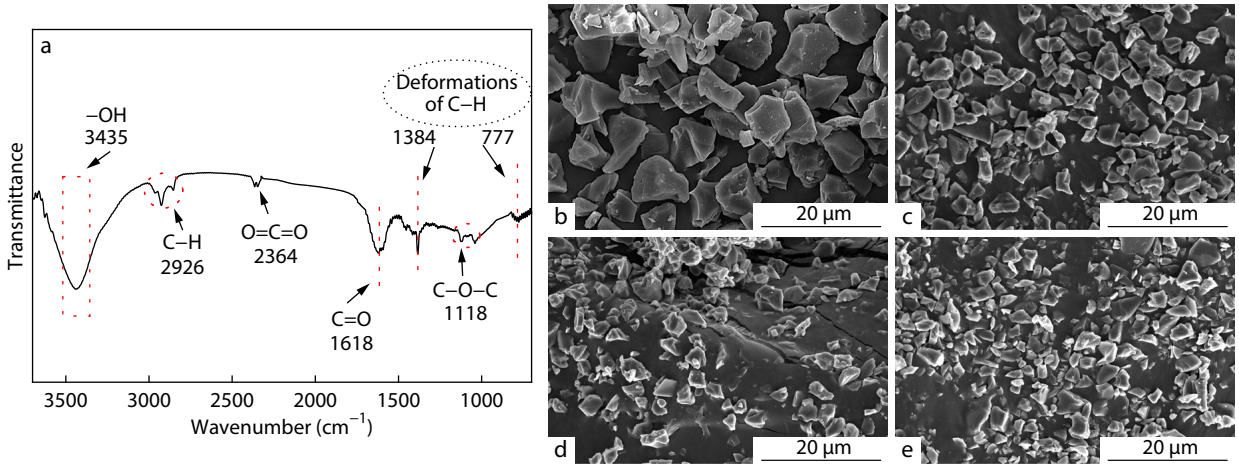

Fig. 2 (a) FTIR spectrum of 1000M BC, and SEM images of BC with different mesh sizes: (b) 100M, (c) 1000M, (d) 2000M, (e) 3000M.

acteristic peaks can be observed at 3435, 2926, 2364, 1618, 1384, 1118, and 777 cm^{-1}. These peaks correspond to the stretching vibrations of hydroxyl groups, C—H bonds, O=C=O bonds, C=O bonds, C—O—C bonds, and deformations of the C—H bonds, respectively. This differs from other carbon materials such as graphene and carbon nanotubes, and the abundance of surface functional groups on BC enhances its potential for performance modification, particularly owing to the presence of carboxyl and carbonyl groups, which improve the compatibility between polymer substrates.[29,30] The SEM images of BC with different particle sizes are shown in Figs. 2(b)–2(e). The particle sizes for various mesh sizes of biochar (100M, 1000M, 2000M, 3000M) were in the range of approximately 2 μm to 12 μm.

Tensile Properties of PVA/PA/BC Composite Films

Fig. 3(A) shows the stress-strain curves of the PVA/PA/BC composite films, while the tensile strength, tensile modulus, and elongation at break are presented in Figs. 3(B)–3(D). The PVA film, as shown in Fig. 3(A), exhibits high brittleness and strength, but limited ductility. Meanwhile, the stress-strain curve for the PVA film reveals two yield points, suggesting that stress yielding occurs due to the tangles between PVA molecule chains, which increases resistance during stretching.

The impact of BC on the reinforcing properties of the PVA composite films is shown in Fig. 3(B). The neat PVA film exhibites high tensile strength (81.8 MPa) and tensile modulus (2.5 GPa), but a relatively low elongation at break (86.5%). When PA was added at 10 wt% content, the tensile strength, tensile modulus and elongation at break of the PVA/PA composite film change to 36.5 MPa, 101 MPa, and 141.4%, respectively. Compared to the counterparts of neat PVA, the tensile strength and tensile modulus of the PVA/PA composite film decrease by 55.4% and 96.0%, respectively. Incorporating BC into the PVA/PA composite films enhances these properties. As the BC content increases from 2 wt% to 10 wt%, the tensile modulus, tensile modulus, and elongation at break of the PVA/PA/BC composite films initially increase and then decrease, with the tensile strength peaking at 2 wt% and the tensile modulus and elongation at break peaking at 5 wt%. Specifically, the PA10/1000BC5 composite film exhibits a tensile modulus of 213 MPa and elongation at break of 281.7%, nearly doubling the values of the PVA/PA composite film. Additionally, the tensile strength is increased by 11.8% compared to the PVA/PA composite film, rising from 36.5 MPa to 40.8 MPa. This may be due to the hydroxyl groups on the surface of BC enhancing the hydrogen bonding network formed by PVA and PA, and at the same time BC could disperse evenly as PA, which reduces the stress concentration and improved the tensile strength of the composite films. However, higher BC content leads to uneven dispersion and agglomeration of BC particles in the PVA matrix, and the hydroxyl groups on the BC surface cannot effectively form hydrogen bonds between PVA and PA, resulting in a weak hydrogen bonding network near the agglomerated BC region. This factor may explain the reduction in the elongation at break observed when the BC content increases from 5 wt% to 8 wt%. This finding is consistent with that of the study by Fu *et al*.[31], who identified 5 wt% BC as an effective toughening agent.

Fig. 3(C) illustrates the effect of BC particle size on the reinforcing properties of the PVA composite films. As the particle size of BC decreases from 100M to 3000M, both tensile strength and elongation at break of the PVA/PA/BC composite films initially increase but then decrease. The peak values for elongation at break (281.7%) and tensile strength (52.9 MPa) are observed for particle sizes of 1000M and 2000M, respectively. The tensile modulus steadily increases from 101 MPa to 529 MPa. The increased surface area of the smaller BC particles improves the stress transfer and enhances the strength and toughness of the composite films. However, excessively small particles tend to agglomerate, which explains the observed decrease in performance at very small particle sizes.[32] Fig. 3(D) shows the impact of PA addition on the tensile properties of the PVA composite films. When 1000M BC was added at 5 wt%, the tensile strength, tensile modulus, and elongation at break of the PVA/BC composite film change to 87.2 MPa, 2660 MPa, and 40.5%, respectively. Compared to the counterparts of neat PVA, the tensile strength and tensile modulus of the PVA/BC composite film increase by 6.6% and 6.1%, respectively. This proves that the addition of BC has a reinforcing effect.[33] Increasing the PA content significantly enhanced the elongation at break of PVA/PA/BC composite films. The elongation at break of PVA/PA/BC composite films initially increased and then decreased with increasing PA content, reaching a peak of 281.7% at 10 wt% of PA, which is a 600% increase compared to PVA/BC composite films. Howev-

https://doi.org/10.1007/s10118-025-3365-z

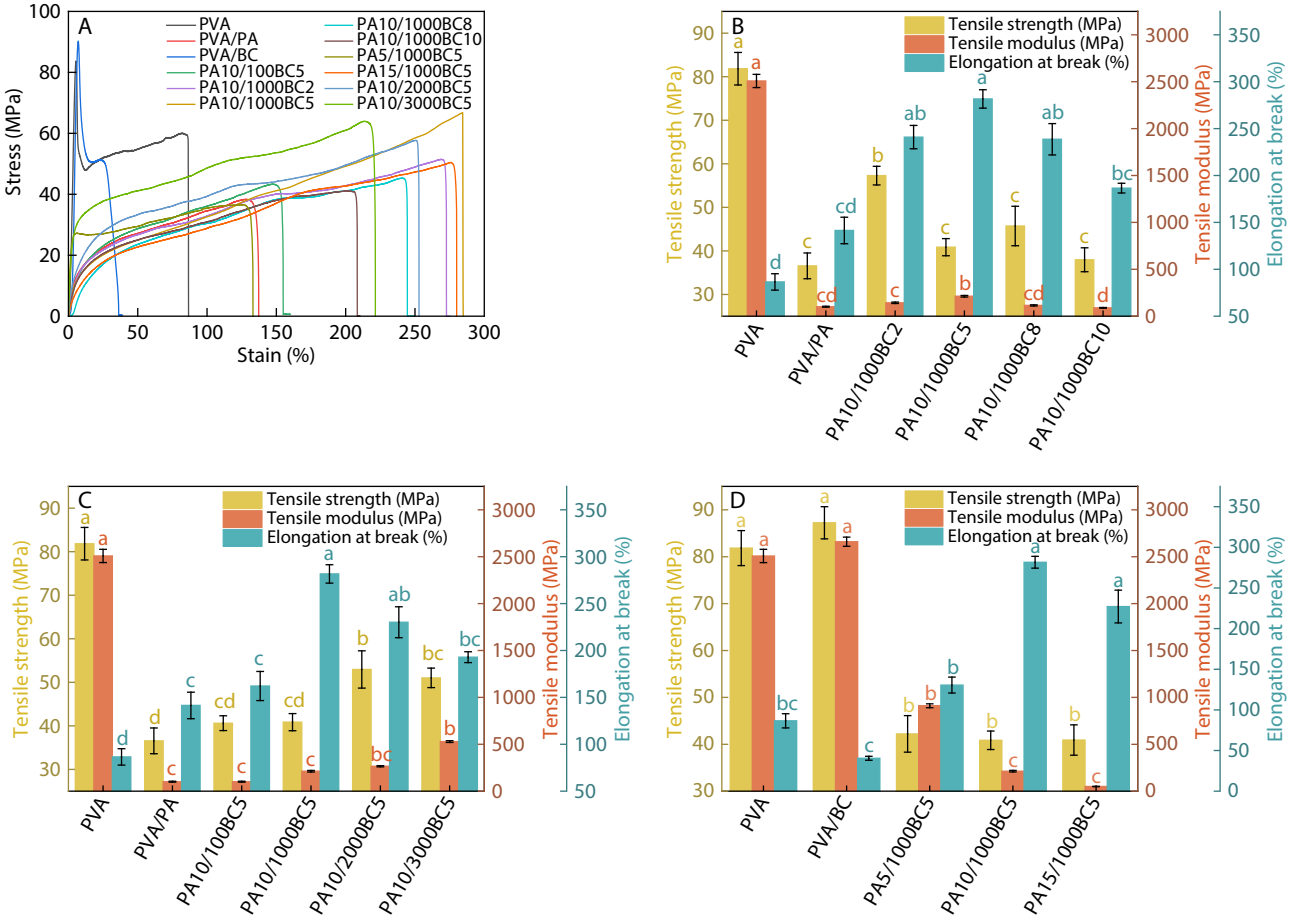

Fig. 3 Tensile properties of PVA composite films: (A) stress-strain curves, (B) BC contents of 2 wt%, 5 wt%, 8 wt% and 10 wt%; (C) BC meshes of 100M, 1000M, 2000M and 3000M; (D) PA contents of 5 wt%, 10 wt% and 15 wt%.

er, this improvement in flexibility comes at the cost of reducing mechanical strength. As the PA content increased, the tensile strength of the composite film decreases from 87.2 MPa (without PA addition) to 40.9 MPa (15 wt% PA addition), while the tensile modulus decreases from 2660 MPa (without PA addition) to 51 MPa (15 wt% PA addition). This tremendous reduction occurs because PA acts as a "plasticizer" that decreases the intermolecular cohesion between PVA chains, facilitating polymer chain movement and making the composite films more flexible during stretching.[34] Meanwhile, excessive plasticization disrupts the cohesive interactions between PVA molecules, resulting in reduced material rigidity and a significant decline in both tensile strength and modulus. Ning *et al.*[35] developed a novel flame-retardant additive for PVA composites by incorporating *N*-(2-hydroxy)-propyl-3-trimethylammonium chitosan chloride and phytic acid. This additive significantly enhanced the elongation at break of the PVA composite film, increasing it from 36.35% to 179.35%. However, it also led to a reduction in tensile strength, from 70.71 MPa to 28.62 MPa. As a result, controlling the PA content can balance the strength and toughness of the PVA/PA/BC composite films.

Micromorphological Feature of PVA/PA/BC Composite Film

Figs. 4(a)–4(f) display the SEM images of both the surface and fractural surface of the PVA/PA/BC composite films. As shown in Figs. 4(a) and 4(b), the pure PVA film features a smooth surface and a relatively flat fracture, indicating low toughness. With the addition of PA, irregular bumps and defects appears on the surface of the material in Figs. 4(c) and 4(d), which may be the reason for the plasticization and decrease in the strength of the composite film. Meanwhile, the appearance of filamentous fracture surface is a typical ductile fracture phenomenon. Uniformly dispersed BC particles appear on the surface of the PVA/PA/BC composite film after adding BC (Figs. 4e and 4f). At the same time, rough and irregular surface morphology as well as filamentous structure appear on the fractural surface, indicating that PVA/PA/BC composite films have excellent ductility and toughness.[36] To investigate the distribution of PA within the PVA matrix, EDS mapping is conducted on the surface of the PA10/1000BC5 composite film, as shown in Fig. 4(e). The characteristic element of P from PA is evenly distributed across the surface, indicating that the PA is well-dispersed within the matrix.

Based on the analysis of the above results and relevant literature, a reasonable explanation of the toughening mechanism is shown in Fig. 4(g). Pure PVA films exhibit a certain tensile strength owing to the entanglement of PVA segments, but lack toughness. With the introduction of PA, these entanglement segments are released and their flowability is im-

proved, thus increasing toughness but reducing strength. BC, as a rigid particle, is uniformly dispersed in the PVA matrix, resisting molecular movement and transmitting stress, thereby achieving particle reinforcement.[37] Simultaneously, the SEM image of the PA10/1000BC5 composite film reveals that BC penetrates the PVA matrix, with its porous structure allowing PVA to penetrate, enhancing compatibility, and ultimately improving both toughness and strength. The FTIR spectra show that the stretching vibrations of the hydroxyl groups of PVA/PA/BC underwent a red shift compared to that of PVA, shifting left from 3436 cm^{-1} to 3441 cm^{-1}, which suggests the formation of hydrogen bonds between the components. Meanwhile, the characteristic peak at 1087 cm^{-1}, corresponding to P—O—C bonds, primarily originates from the functional groups in PA. This may also have resulted from the esterification reaction between PVA and PA, as illustrated in the re-

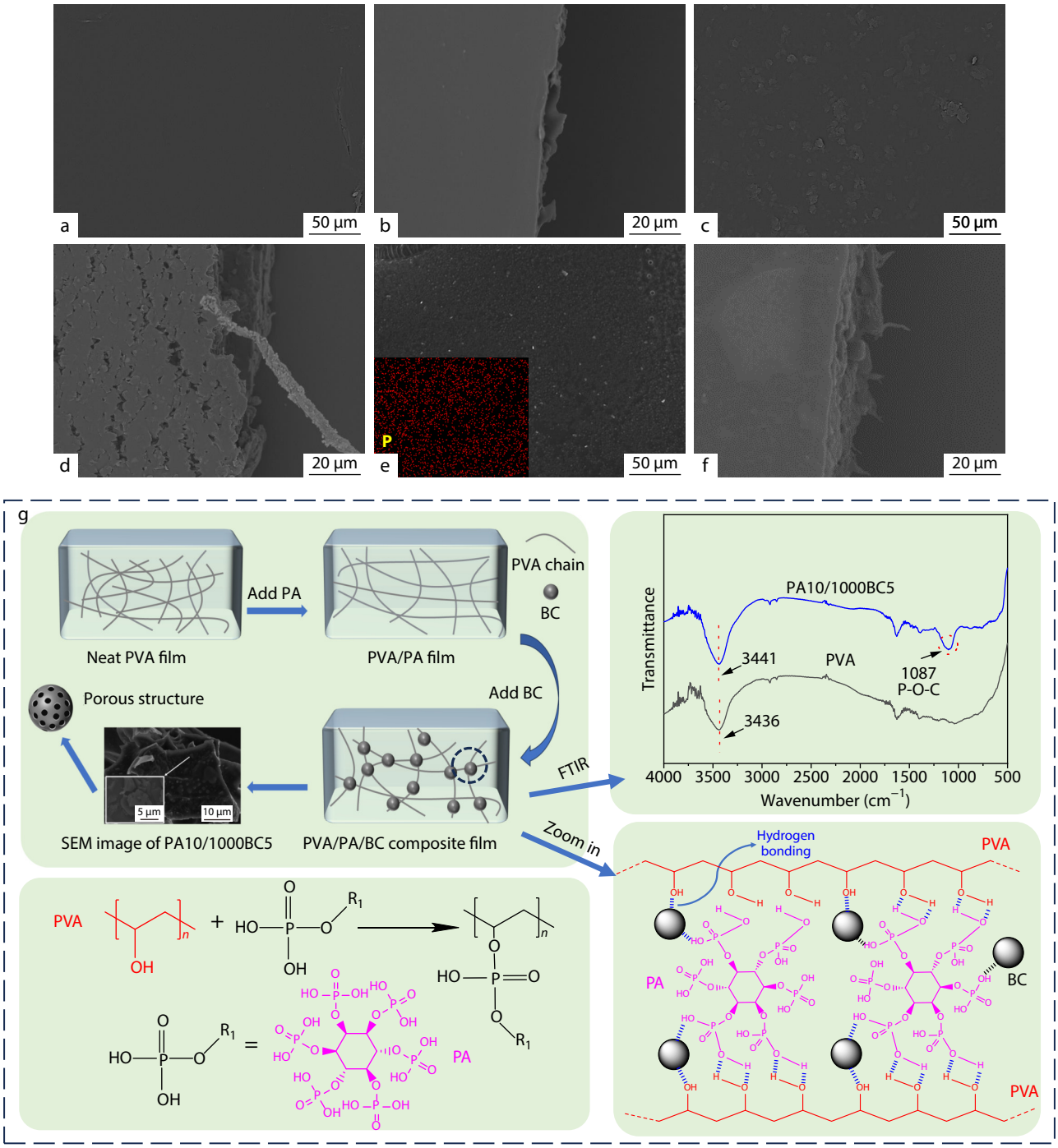

Fig. 4 SEM images of PVA film and PVA/PA/BC composite films: (a) PVA surface, (b) PVA fractural surface, (c) PVA/PA composite surface, (d) PVA/PA composite fractural surface, (e) PA10/1000BC5 composite surface and EDS mapping of phosphorus element, (f) PA10/1000BC5 composite fractural surface. (g) Schematic diagram of toughening mechanism and FTIR spectra of PVA/PA/BC composite films.

https://doi.org/10.1007/s10118-025-3365-z

action diagram in Fig. 4(g). The addition of PA increased the toughness but decreased the strength of the PVA composite film, whereas the addition of BC increased the strength but decreased the toughness of the PVA composite film. However, the synergistic effect of PA and BC enhanced the hydrogen bonding network between PA, BC, and PVA, resulting in composite films with high toughness while maintaining sufficient strength. These facts are crucial for advancing the application of flame-retardant PVA materials in specialized fields.

Thermal Analysis of PVA/PA/BC Composite Films

Fig. 5 presents the TGA and DTG curves of PVA composite films with different PA and BC additions. The thermal degradation data are shown in Table 2, including the initial degradation temperature ($T_{10\%}$), the temperatures of maximum degradation rate (T_{max1} and T_{max2}), and mass residue at 600 °C. The weight loss observed between 80 °C and 120 °C for all the films was due to the evaporation of bound and free water. Pure PVA film exhibits two main degradation stages at 324.5 and 407.9 °C. For the PVA/BC composite film, these stages occur at 322.2 and 397.9 °C. PVA/PA and PVA/PA/BC composite films containing 10 wt% PA also exhibited two degradation processes. However, these processes occur at approximately 230 and 430 °C. The addition of PA lowered the $T_{10\%}$ from 272.2 °C to 180 °C and shifted the T_{max1} from 324.5 °C to 230 °C. This reduction was attributed to the catalytic decomposition effect of the phosphorus groups present in PA. The early decomposition creates a carbon layer that protects the remaining material during combustion.[38] The T_{max2} of the PVA/PA/BC composite film increases from 407.9 °C to 430 °C, likely due to the formation of a protective carbon layer resulting from the PA's catalytic action, which enhances the thermal stability and protects the remaining PVA.[39]

Simultaneously, as the amount of BC added increased from 2 wt% to 10 wt%, the mass residue at 600 °C increased. At the same time, the $T_{10\%}$ initially decreased and then increased, whereas the T_{max1} and the T_{max2} initially increased and then decreased, all reaching their maximum values at a BC dosage of 5 wt%. The addition of 5 wt% BC facilitated the early decomposition of PA10/1000BC5 composite, which promoted the formation of a dense carbon layer. This carbon layer, stabilized in a nitrogen atmosphere, acted as a protective barrier for the PVA matrix, thereby enhancing the thermal stability of the composite film.[40]

As the particle size of BC ranges from 100M to 3000M, the thermal properties of the PVA composite films are initially strengthened and then weakened. The optimal thermal stability performance was found when the BC mesh number was 1000M, with the T_{max1} and residual carbon rate of 234.2 °C and 21.90%, respectively. This may be due to the difficulty of achieving uniform dispersion when the BC particle size is too large (100M), and agglomeration occurred when the particle size was too small (3000M), which was not conducive to the formation of a uniform and dense carbon layer.

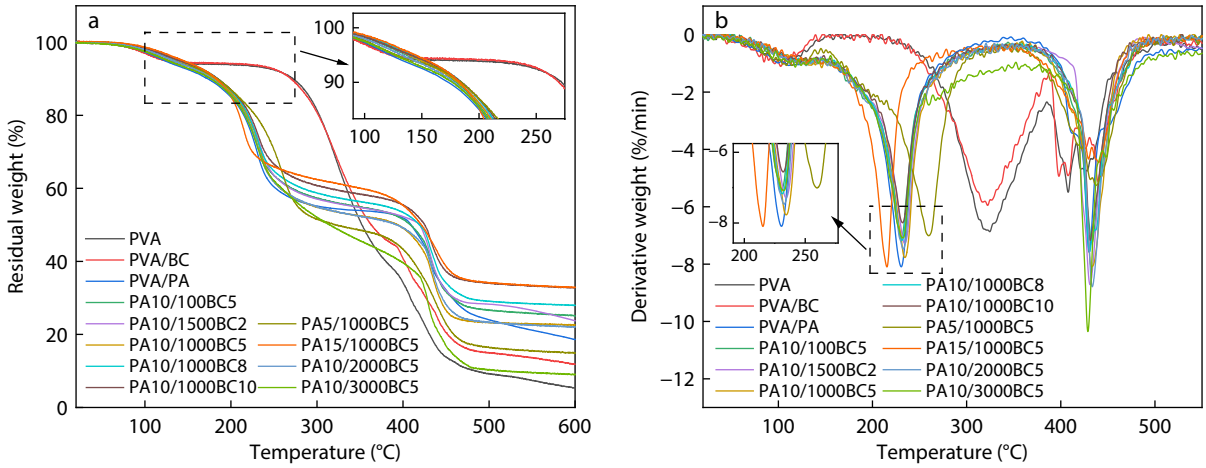

Fig. 5 Thermal stability of PVA/PA/BC composite films: (a) TGA and (b) DTG curves.

Table 2 Thermal performance parameters of composite films of PVA/PA/BC composite films.

Sample	$T_{10\%}$ (°C)	T_{max1} (°C)	T_{max2} (°C)	Mass residue at 600 °C (%)
PVA	272.2	324.5	407.9	4.56
PVA/BC	270.0	322.2	397.9	10.72
PVA/PA	173.2	230.9	429.9	17.18
PA10/100BC5	180.7	230.1	433.2	24.91
PA10/1000BC2	182.1	234.2	430.7	21.90
PA10/1000BC5	181.5	234.4	432.5	22.56
PA10/1000BC8	184.8	231.3	430.6	27.73
PA10/1000BC10	184.7	231.9	431.2	32.38
PA5/1000BC5	183.8	259.6	437.7	14.75
PA15/1000BC5	182.9	215.3	440.3	32.66
PA10/2000BC5	178.1	232.6	433.4	21.78
PA10/3000BC5	176.3	232.5	428.8	8.80

https://doi.org/10.1007/s10118-025-3365-z

Furthermore, with the addition of 5 wt% 1000 mesh BC and an increase in PA content by 5 wt%, 10 wt%, and 15 wt%, the T_{max1} of the composite films decreased (*i.e.* 259.6, 234.2, 215.3 °C). The residual char yields (14.75%, 21.90%, 32.66%) steadily increased, exhibiting relative increases of 323%, 480%, and 716% compared to the 4.56% of pure PVA. The substantial increase of PA amount introduced a significant number of phosphorus-containing groups, making the catalytic degradation effect more pronounced.[41] The carbon layers formed from PA decomposition can protect the PVA matrix from thermal degradation, thereby enhancing its flame retardancy. This effect will be confirmed during combustion analysis.

Flame Retardancy and Its Mechanism of PVA/PA/BC Composite Films

The specific detailed results of the LOI tests are presented in Table 3, and screenshots of the vertical burning test videos are shown in Fig. 6 The vertical combustion process of PVA composite films are shown in Movies S1–S4 (in the electronic supplementary information, ESI). As shown in Fig. 6(a), the pure PVA film exhibited molten droplets during the combustion process at 22 s, and these molten droplets, accompanied by flames, quickly ignited the absorbent cotton. Meanwhile, the LOI of the pure PVA film was only 18.4%, and it could not achieve any rating in the UL-94 test, indicating that PVA is flammable. Meanwhile, the LOI of the PVA/BC composite film increased slightly from 18.4% to 20.1% compared to that of the pure PVA film (Fig. 6b), but still failed to attain a rating in the UL-94 test. The rapid ignition of the dripping molten droplets after ignition quickly ignites the cotton, which can lead to the spread of fire in actual fire incidents, resulting in devastating disasters. However, comparing the PVA/PA/BC composite films with different amounts of added PA (5 wt%, 10 wt%, and 15 wt%), the LOI values were 31.5%, 39.2%, and 42.1%, respectively. Notably, in the UL-94 test, no molten droplets were observed, and the composite films achieved the V-0 rating. Compared to the PVA/BC composite film, the LOI of the PA5/1000BC10 composite film with 5 wt% PA exhibited a significant increase from 20.1% to 31.5%. Furthermore, the composite film achieved the V-0 rating. In addition, the PVA composite films with PA exhibited excellent self-

Table 3 Key data of PVA/PA/BC composite films from vertical burning text and LOI test.

Samples	LOI (%)	Vertical burning test		
		t_1/t_2	Dripping/Ignition of cotton	Rating
PVA	18.4 ± 0.2	>30	Yes/Yes	NR
PVA/BC	20.1 ± 0 2	>30	Yes/Yes	NR
PVA/PA	36.0 ± 0.1	1.5/1.6	No/No	V-0
PA5/1000BC5	31.5 ± 0.3	1.7/2.1	No/No	V-0
PA10/1000BC5	39.2 ± 0.1	1.5/1.6	No/No	V-0
PA15/1000BC5	42.1 ± 0.2	1.2/1.4	No/No	V-0

Note: t_1 represents the burning duration of the first ignition, and t_2 represents the burning duration of the second ignition.

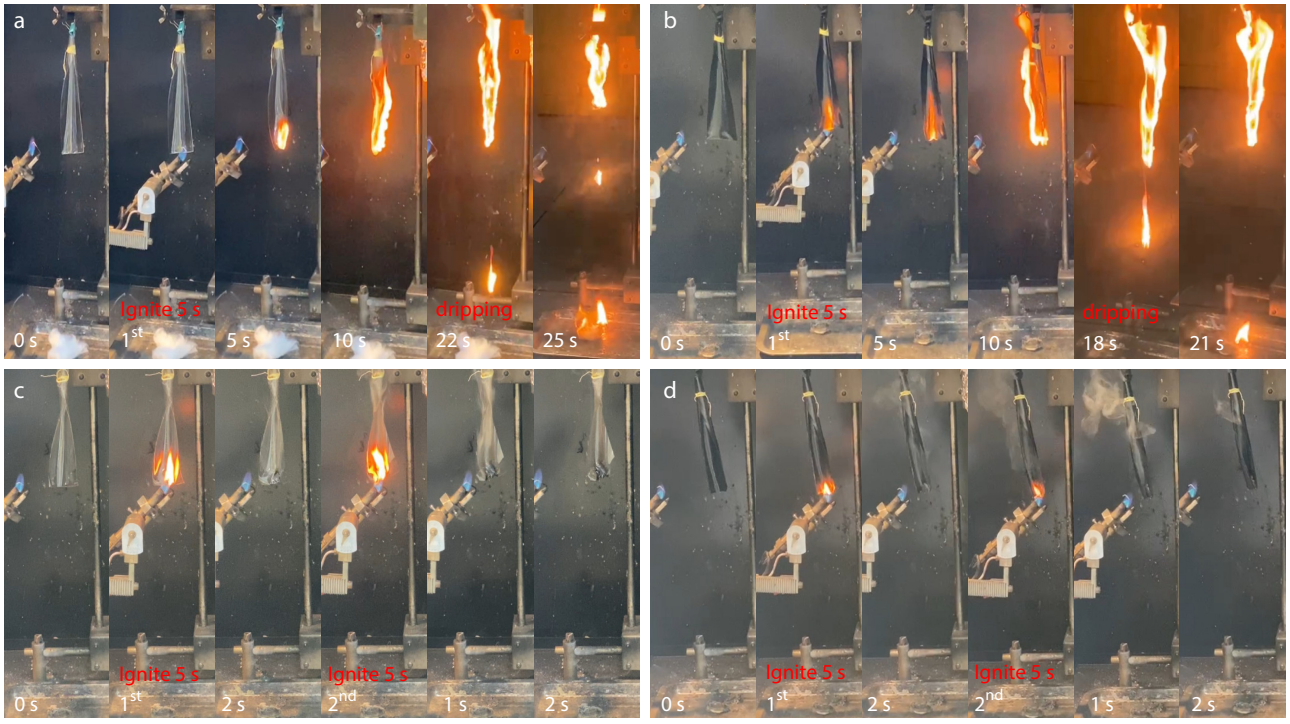

Fig. 6 Video screenshots from UL-94 tests of (a) PVA film, (b) PVA/BC composite film, (c) PVA/PA composite film, and (d) PA10/1000BC5 composite film.

https://doi.org/10.1007/s10118-025-3365-z

extinguishing capabilities, as presented in Table 3. When the samples were removed from the flame, they extinguished in less than 2 s. This indicates that the addition of PA improves the flame-retardant performance of PVA composite films, and the effect becomes more pronounced with increasing amounts of added PA. Furthermore, comparing the PVA/PA composite films with the PA10/1000BC5, it is evident that the addition of BC results in an increase in the LOI of the composite film from 31.5% to 36.0%. This indicates that the addition of BC may synergistically enhance the flame-retardant modification provided by PA in PVA composite films.

The combustion behavior of the PVA composites was also evaluated using cone calorimetry. Figs. 7(a) and 7(b) show the heat release rate (HRR) and total heat release (THR) curves. Additionally, key data from the CCT, such as time to ignition (TTI), peak heat release rate (pHRR), THR, residual mass, and total smoke release (TSR) are provided in Table 4. The pure PVA film exhibited high flammability with pHRR and THR of 186 kW/m^2 and 3.33 MJ/m^2, respectively, whereas the pHRR and THR of the PVA/BC composite film with the addition of 5 wt% 1000 mesh BC remains unchanged in comparison to the pure PVA. After adding PA, the TTI of the PVA/PA composite film decreased from 12 s to 9 s. The introduction of PA promoted the early decomposition of the PVA/PA/BC composite film, while pHRR and THR decreased to 83 kW/m^2 and 1.52 MJ/m^2. Notably, the residual mass of the PA10/1000BC5 composite film reached 30.6% and the TTI was 2 s faster than that of the PVA/PA composite film.

The TSR data were used to assess the smoke suppression effect of the developed flame retardant on PVA films. The pure PVA exhibited a TSR value of 46.2. After the addition of PA, the TSR of the PVA/PA composite film significantly to 89.1. This is because PA can promote the carbonization of PVA, which leads to the incomplete combustion of PVA, generat-

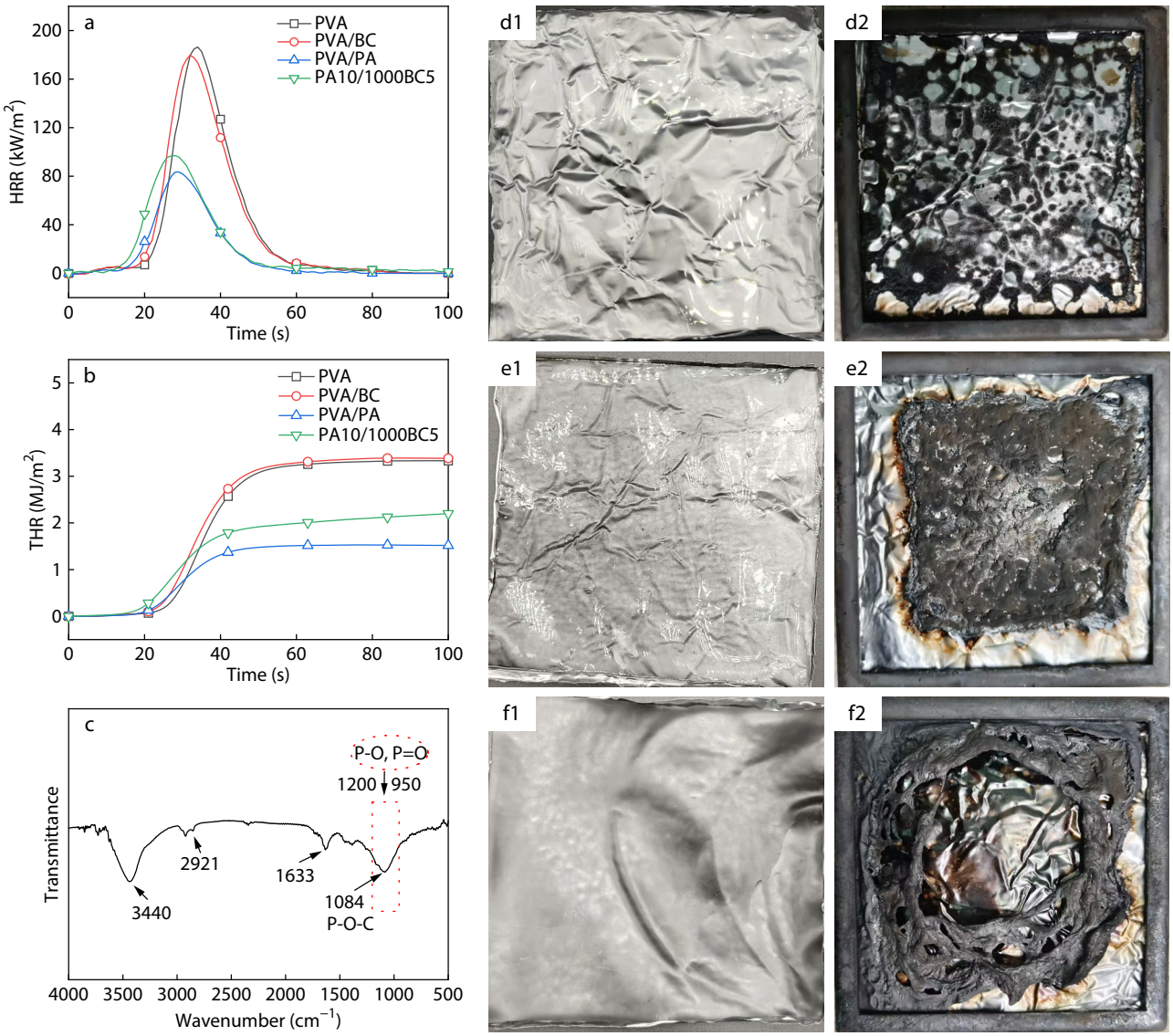

Fig. 7 (a) HRR and (b) THR curves of PVA, PVA/BC, PVA/PA and PA10/1000BC5; (c) FTIR spectrum of residual carbon from PA10/1000BC5 composite film after combustion; (d1–f2) Digital photographs of composite films before CCT (d1, PVA/BC composite film; e1, PVA/PA composite film; f1, PA10/1000BC5 composite film) and after CCT (d2, PVA/BC composite film; e2, PVA/PA composite film; f2, PA10/1000BC5 composite film).

https://doi.org/10.1007/s10118-025-3365-z

Table 4 Key data of PVA/PA/BC composite films from CCT.

Sample	TTI (s)	pHRR (kW/m^2)	THR (MJ/m^2)	Residual mass (wt%)	TSR (m^2/m^2)
PVA	12 ± 1	186 ± 4	3.3 ± 0.1	0 ± 0.1	46.2 ± 0.2
PVA/BC	14 ± 1	179 ± 2	3.4 ± 0.1	12.5 ± 2.0	37.1 ± 0.6
PVA/PA	9 ± 1	83 ± 3	1.5 ± 0.3	17.8 ± 0.5	89.1 ± 1.3
PA10/1000BC5	7 ± 1	97 ± 1	2.2 ± 0.2	30.6 ± 1.0	78.1 ± 0.5

ing more smoke.[42] Conversely, incorporating BC reduces the TSR, the comparison between PVA and PVA/BC (46.2 to 37.1), as well as between PVA/PA and PA10/1000BC5 (89.1 to 78.1). The reason may be that the combination of PA and BC increases the density and continuity of the generated carbon layer denser and more continuous, which protects the PVA substrate from flame erosion and inhibits smoke release. The porous structure of BC has a certain adsorption effect on smoke.

From the FTIR spectra of the residual carbon of the PA10/1000BC5 composite film after combustion in Fig. 7(c), it can be seen that the P—O—C asymmetrical stretching occurs at 1084 cm^{-1}, and the stretching vibrations of P—O and P=O exist in the range of 1200 cm^{-1} to 950 cm^{-1}. This indicates the successful introduction of PA into the PVA/PA/BC composite films, while the phosphate groups in PA were involved in the formation of the carbon layer. Digital photographs of the composite films after CCT are shown in Figs. 7(d2)–7(f2), it can be seen that the residual carbon of the PVA/BC composite film is mainly in the form of dispersed carbon powder, while the residual carbon of the PVA/PA and PA10/1000BC5 composite films formed a continuous carbon layer.

The surface features of the PA10/1000BC5 composite film before and after combustion are shown in Figs. 8(a) and 8(b). The surface transitioned from smooth to rough and uneven. In addition, irregular and thick carbon layers appeared on the surface after combustion. Based on the above detailed analysis and relevant literatures,[43] a reasonable speculation on the flame-retardant mechanism is presented in Fig. 8(c). First, PA undergoes thermal decomposition to produce free radicals, including PO· and HPO·, which can trap H· and HO· free radicals in the combustion gas phase[44] and the polyphosphoric acid generated by PA decomposition promotes the carbon layer. Additionally, inert gases, such as CO_2 and H_2O, are generated, which block the transfer of heat and oxygen.[45] Simultaneously, BC acts as a high-quality carbon source that synergistically enhances the formation of the carbon layer during the process facilitated by PA.[23] This results in the formation of a thick carbon layer, effectively impeding the exchange of heat between the flame and the substrate.[46] The synergistic effect of PA and BC allowed the PVA/PA/BC composite film to form a more continuous and thicker carbon layer to protect the PVA substrate during combustion, with PA acting as the main flame retardant and BC acting as the carbon source. Ultimately, these facts contribute to the improvement of the flame-retardant performance of PVA composites.

Hydrophilicity

Figs. 9(a) and 9(b) show the hydrophilicity of pure PVA and PVA/PA/BC composite films. The water contact angle and swelling ratio of PVA/PA/BC composite films are related to their water sensitivity, both immediate and sustained.[47] The pure PVA film, PVA/PA composite film, and PVA/BC composite film dissolve in water within 6 h, and thus no swelling ratio data is available. On the contrary, the PVA/PA/BC composite films maintain their integrity without dissolving, which shows that PA and BC improve the water resistance of PVA. Similar results were reported by Zhang *et al.*[48] and Xia *et al.*[49]. They attributed the

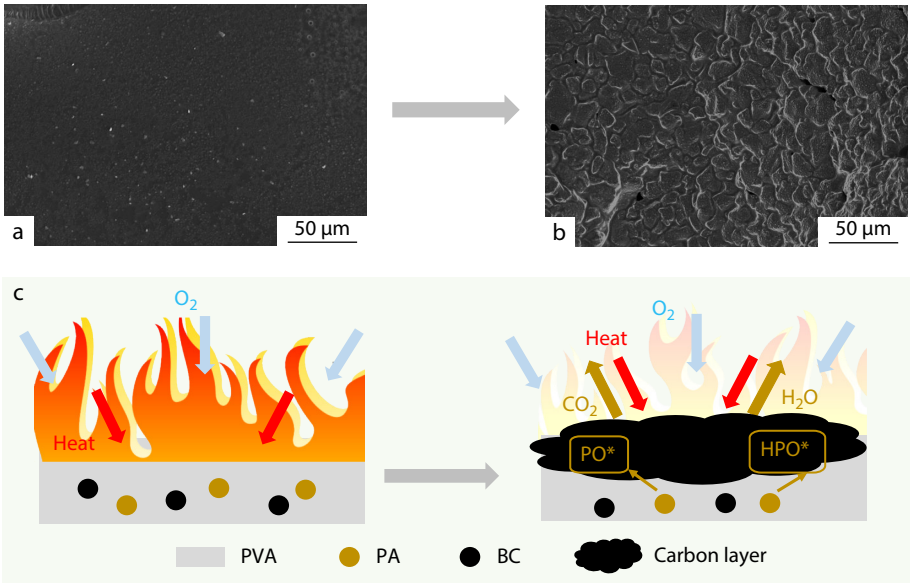

Fig. 8 SEM image of PA10/1000BC5 composite film surface before (a) and after (b) combustion, and the schematic diagram of flame retardancy mechanism of PVA/PA/BC composite films (c).

https://doi.org/10.1007/s10118-025-3365-z

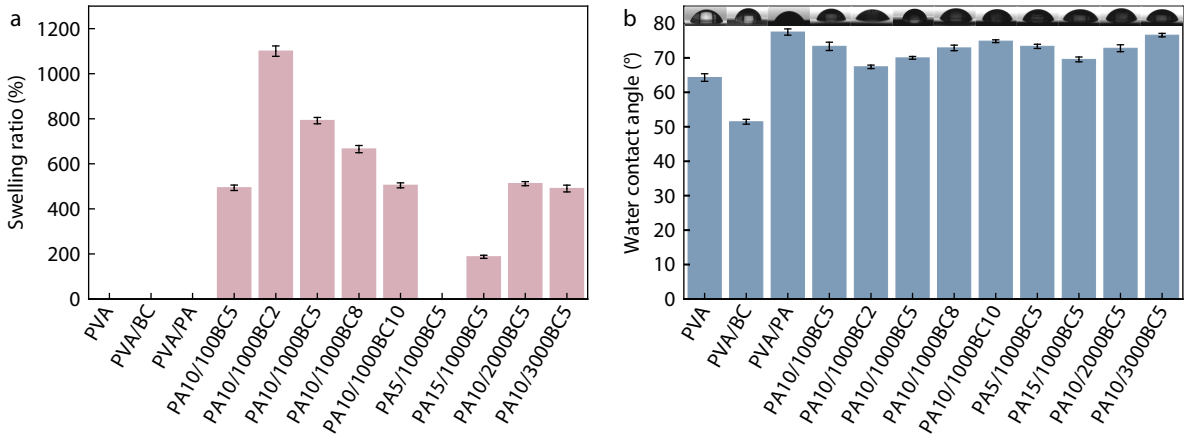

Fig. 9 (a) Swelling ratio after immersion and (b) water contact angle of PVA composite films. Note: Some swelling ratio values were missing because the composite films were dissolved in deionized water and could not be measured.

formation of strong hydrogen bonds between the matrix and the filler. Therefore, the synergistic effect of PA and BC not only enhanced the hydrogen bonding network within the PVA/PA/BC composite films but also conferred a certain degree of rigidity to the hydrogen bonding network, which resulted in improved resistance to swelling. The water contact angle data showed that all the composite films had good hydrophilic properties. Notably, the PVA/BC composite film with 5 wt% 1000M BC had the lowest contact angle at 51.4°, a decrease of 12.9° compared to the 64.3° of pure PVA. This may be due to the addition of BC, which disrupts the uniformity of the PVA film surface, leading to an increase in the contact angle. Additionally, adding PA to the PVA film increased the contact angle to 77.5°, which is a 13.2° increase compared to that of pure PVA. As mentioned earlier, PA and PVA may form ester bonds, which can lead to an increase in the contact angle. However, the composite films maintained their hydrophilic nature.

As the BC content increased from 2 wt% to 10 wt%, the swelling ratio of the PVA/PA/BC composite films (with 10 wt% PA addition) decreased, while the water contact angle increased. This may be attributed to the hydroxyl groups on the BC surface promoting the formation of a hydrogen bond network between PVA and PA, which enhances the water resistance inside the film and reduces the exposure of the hydroxyl groups on the surface, thereby increasing the contact angle.[50] The swelling ratio of PVA/PA/BC composite films (with 10 wt% PA added) initially increased and then decreased as the BC mesh size increases from 100M to 3000M, peaking at 791.8% with the 1000M mesh size. This effect may be attributed to the more effective dispersion of the 1000M biochar, which facilitates the formation of additional hydrogen bonds between PA and PVA. Consequently, the composite could adsorb a greater amount of water. Furthermore, the contact angles of the PVA/PA/BC composite films were all approximately 73°, except for the PA10/3000BC5 composite film, indicating that the strength of the hydrogen-bonding network is largely affected by the size of the BC particles. The PA10/3000BC5 composite film may have increased the water contact angle to 76.8° owing to the aggregation of the BC particles.[32] Because the hydrogen bond network near the agglomerated BC regions is weaker, leading to lower hydrophilicity.

The addition of PA primarily influenced the strength of the hydrogen-bonding network within the composite film, thereby affecting its water resistance.[51] As the PA content increased to 15 wt%, the swelling decreased to 187.2%. However, when the PA content was only 5 wt%, the PA5/1000BC5 composite film dissolved because of the insufficient hydrogen bond strength. Consequently, the combination of PA and BC enhanced the hydrogen-bonding network within the PVA/PA/BC composite film, resulting in improved swelling resistance. Therefore, controlling the amount of PA and BC is crucial for producing PVA/PA/BC composite films that strike a balance between hydrophilicity and water sensitivity, which is essential for the long-term performance of PVA in humid environments.

CONCLUSIONS

In this study, a novel green flame-retardant system incorporating PA and BC into PVA was developed, endowing the PVA composite films with outstanding flame retardancy, good flexibility, thermal stability, and water stability. The synergistic effect of PA and BC imparts flame retardant properties to PVA composite films, concurrently raising the LOI to above 30% and achieving a V-0 rating in the UL-94 test. This result meets international standards for flame retardant plastics. In terms of mechanical properties, the addition of PA enhanced the toughness of the composite film but led to a reduction in strength. However, the uniform dispersion of biochar particles countered this effect, providing reinforcement that improved the flexibility of the PVA composite films while preserving adequate strength. Notably, the PA10/1000BC5 composite film containing 5 wt% 1000M BC and 10 wt% PA demonstrated a remarkable 281.7% increase in elongation at break. Additionally, the tensile modulus increased to 52.1 MPa, and the tensile strength reached 40.9 MPa. The hydrogen bonding network between PA, BC, and PVA helps maintain the hydrophilic properties of the PVA/PA/BC composite films while enhancing their water resistance. The significance of this research lies not only in providing a new approach to enhance the flame retardancy of PVA, but also in laying the groundwork for the development of more environmentally friendly and sustainable flame-retardant materials.

https://doi.org/10.1007/s10118-025-3365-z

Conflict of Interests

The authors declare no interest conflict.

Electronic Supplementary Information

Electronic supplementary information (ESI) is available free of charge in the online version of this article at http://doi.org/10.1007/s10118-025-3365-z.

Data Availability Statement

The data that support the findings of this study are available from the corresponding author upon reasonable request.

ACKNOWLEDGMENTS

This work was financially supported by the Zhejiang Provincial "Vanguard" and "Leading Goose" R&D Program (No. 2025C02203), the Zhejiang Provincial Natural Science Foundation of China (No. LTGS24C130001), the Fund for Key Scientific Research in the Public Interest of Ningbo (No. 2024S009).

REFERENCES

1 He, W.; Song, P.; Yu, B.; Fang, Z.; Wang, H. Flame retardant polymeric nanocomposites through the combination of nanomaterials and conventional flame retardants. *Prog. Mater. Sci.* **2020**, *114*, 100687.
2 Zhong, B.; Jiang, J.; Yao, S.; Li, J.; Luo, X.; Jia, Z. Thermally stable, mechanically strong, easily biodegradable and water-resistant poly(vinyl alcohol) composites crosslinked by supported crosslinker. *Compos. Sci. Technol.* **2024**, *248*, 110427.
3 Tan, W.; Gao, L.; Su, J.; Zuo, C.; Ren, Y.; Liu, X. Phosphonitrile-modified biomass multi-crosslinking strategy: Construction of flame retardant, smoke suppressive and antibacterial polyvinyl alcohol composites. *Compos. Part A-Appl. Sci. Manuf.* **2024**, *177*, 107897.
4 Wan, M.; Shi, C.; Qian, X.; Qin, Y.; Jing, J.; Che, H.; Ren, F.; Li, J.; Yu, B.; Zhou, K. Design of novel double-layer coated ammonium polyphosphate and its application in flame retardant thermoplastic polyurethanes. *Chem. Eng. J.* **2023**, *459*, 141448.
5 Joulaei, M.; Hedayati, K.; Ghanbari, D. Investigation of magnetic, mechanical and flame retardant properties of polymeric nanocomposites: Green synthesis of $MgFe_2O_4$ by lime and orange extracts. *Compos. Part B-Eng.* **2019**, *176*, 107345.
6 Khalili, P.; Liu, X.; Tshai, K. Y.; Rudd, C.; Yi, X.; Kong, I. Development of fire retardancy of natural fiber composite encouraged by a synergy between zinc borate and ammonium polyphosphate. *Compos. Part B-Eng.* **2019**, *159*, 165–172.
7 Zuo, C.; Liu, Y.; Guo, Y.; Tan, W.; Ren, Y.; Liu, X. Preparation of a copper porphyrin derivative and its surface modification for simultaneously endowing PET fibers with dyeing, flame retardant and anti-dripping performance. *Polym. Degrad. Stabil.* **2023**, *209*, 110273.
8 Chen, X.; Tang, Z. Ultra-high thermal conductivity FGN/PVA/MXene composite films with good electrical insulation. *Compos. Sci. Technol.* **2023**, *242*, 110208.
9 Wang, X.; Guo, W.; Cai, W.; Wang, J.; Song, L.; Hu, Y. Recent advances in construction of hybrid nano-structures for flame retardant polymers application. *Appl. Mater. Today* **2020**, *20*, 100762.
10 Zhang, M.; Chen, H. Development and characterization of starch-sodium alginate-montmorillonite biodegradable antibacterial films. *Int. J. Biol. Macromol.* **2023**, *233*, 123462.
11 Ahmadian-Fard-Fini, S.; Ghanbari, D., Salavati-Niasari, M. Photoluminescence carbon dot as a sensor for detecting of Pseudomonas aeruginosa bacteria: Hydrothermal synthesis of magnetic hollow NiFe2O4-carbon dots nanocomposite material. *Compos. Part B-Eng.* **2019**, *161*, 564–577.
12 Amiri, M.; Salavati-Niasari, M.; Akbari, A. Magnetic nanocarriers: Evolution of spinel ferrites for medical applications. *Adv. Colloid Interface Sci.* **2019**, *265*, 29–44.
13 Yang, Y.; Wang, D. Y.; Haurie, L.; Liu, Z.; Zhang, L. Combination of corn pith fiber and biobased flame retardant: a novel method toward flame retardancy, thermal stability, and mechanical properties of polylactide. *Polymers* **2021**, *13*, 1562.
14 Azizi, S.; Ahmad, M. B.; Ibrahim, N. A.; Hussein, M. Z.; Namvar, F. Preparation and properties of poly(vinyl alcohol)/chitosan blend bio-nanocomposites reinforced by cellulose nanocrystals. *Chinese J. Polym. Sci.* **2014**, *32*, 1620–1627.
15 Qiu, S.; Li, Y.; Qi, P.; Meng, D.; Sun, J.; Li, H.; Cui, Z.; Gu, X.; Zhang, S. Improving the flame retardancy and accelerating the degradation of poly (lactic acid) in soil by introducing fully bio-based additives. *Int. J. Biol. Macromol.* **2021**, *193*, 44–52.
16 Chen, Y.; Yao, J.; Xu, M. K.; Jiang, Z. G.; Zhang, H. B. Electrically conductive and flame retardant graphene/brominated polystyrene/maleic anhydride grafted high density polyethylene nanocomposites with satisfactory mechanical properties. *Chinese J. Polym. Sci.* **2019**, *37*, 509–517.
17 Liu, Y.; Chen, Y.; Qi, H. Recyclable cellulose nanofibers reinforced poly(vinyl alcohol) films with high mechanical strength and water resistance. *Carbohydr. Polym.* **2022**, *293*, 119729.
18 Zhang, N.; Zhang, B.; Pang, Y.; Yang, H. S.; Zong, L.; Duan, Y. X.; Zhang, J. M. High performance of PVA nanocomposite reinforced by Janus-like asymmetrically oxidized graphene: synergetic effect of H-bonding interaction and interfacial crystallization. *Chinese J. Polym. Sci.* **2022**, *40*, 373–383.
19 Li, Z.; Li, Y.; Shen, Y.; Yu, T.; Wang, J. Synergic effects of dimethyl methylphosphonate (DMMP) and nano-sized montmorillonite (MMT) on the flammability and mechanical properties of flax fiber reinforced phenolic composites under hydrothermal aging. *Compos. Sci. Technol.* **2022**, *230*, 109487.
20 Li, W.; An, J.; Lu, Y.; Li, S. Effects of PVA fibers and multi-walled carbon nanotubes reinforcement on uniaxial compression fatigue properties of Engineered geopolymer composites. *Compos. Struct.* **2024**, *337*, 118028.
21 Zouari, M.; Stanciu, S. G.; Jakes, J.; Marrot, L.; Fiorentis, E.; Stanciu, G. A.; DeVallance, D. A. et al. Investigations on the topography and micro-mechanical properties of polyvinyl alcohol thin-film composites reinforced with hardwood biocarbon particles. *J. Mater. Res. and Technol.* **2023**, *27*, 5533–5540.
22 Zhong, X.; Pan, Y.; Feng, Z.; Shao, Z. B.; Qiu, J.; Zhu, L. Rice straw-based cellulose nanofiber reinforcing polyvinyl alcohol antibacterial film through electrospinning. *Compos. Commun.* **2024**, *49*, 101972.
23 Mozrall, A. M.; Hernandez-Charpak, Y. D.; Trabold, T. A.; Diaz, C. A. Effect of biochar content and particle size on mechanical properties of biochar-bioplastic composites. *Sustain. Chem. Pharm.* **2023**, *35*, 101223.
24 Barbalini, M.; Bartoli, M.; Tagliaferro, A.; Malucelli, G. Phytic acid and biochar: an effective all bio-sourced flame retardant formulation for cotton fabrics. *Polymers* **2020**, *12*, 811.

25 Jagdale, P.; Ziegler, D.; Rovere, M.; Tulliani, J. M.; Tagliaferro, A. Waste coffee ground biochar: a material for humidity sensors. *Sensors* **2019**, *19*, 801.

26 Kong, Y.; Qian, S.; Zhang, Z.; Tian, J. The impact of esterified nanofibrillated cellulose content on the properties of thermoplastic starch/PBAT biocomposite films through ball-milling. *Int. J. Biol. Macromol.* **2023**, *253*, 127462.

27 Gu, Q.; Zhu, C.; Cheng, R.; Zhou, J.; He, J.; Liu, T.; Yang, Y.; Lian, Y.; Zhang, K. Formation mechanism of a novel core-shell with tetradecyl dimethyl benzyl ammonium–modified montmorillonite interlayer nanofibrous membrane and its antimicrobial properties. *Colloids Surf. B* **2024**, *238*, 113889.

28 Zhang, Z.; Qian, S.; Li, X.; Zhu, C.; Li, Z. Preparation of environmentally friendly ionic liquids-toughened polylactic acid/nanofibrillated cellulose composites with high strength and precipitation resistance. *Chem. Eng. J.* **2024**, *499*, 156670.

29 Usman, A.; Hussain, Z.; Riaz, A.; Khan, A. N. Enhanced mechanical, thermal and antimicrobial properties of poly(vinyl alcohol)/graphene oxide/starch/silver nanocomposites films. *Carbohydr. Polym.* **2016**, *153*, 592–599.

30 Qian, S.; Kong, Y.; Cheng, H.; Tu, S.; Zhai, C. Interfacial interaction improvement of polylactic acid/bamboo-char biocomposites for high toughness, good strength, and excellent thermal stability. *Surf. Interfaces.* **2023**, *42*, 103315.

31 Fu, S. Y.; Feng, X. Q.; Lauke, B.; Mai, Y. W. Effects of particle size, particle/matrix interface adhesion and particle loading on mechanical properties of particulate–polymer composites. *Compos. Part B-Eng.* **2008**, *39*, 933–961.

32 Zare, Y.; Rhee, K. Y.; Hui, D. Influences of nanoparticles aggregation/agglomeration on the interfacial/interphase and tensile properties of nanocomposites. *Compos. Part B-Eng.* **2017**, *122*, 41–46.

33 Giorcelli, M.; Bartoli, M. Development of coffee biochar filler for the production of electrical conductive reinforced plastic. *Polymers* **2019**, *11*, 1916.

34 Liang, B.; Jiang, Q.; Tang, S.; Li, S.; Chen, X. Porous polymer electrolytes with high ionic conductivity and good mechanical property for rechargeable batteries. *J. Power Sources* **2016**, *307*, 320–328.

35 Ning, Y.; Liu, R.; Chi, W.; An, X.; Zhu, Q.; Xu, S.; Wang, L. A chitosan derivative/phytic acid polyelectrolyte complex endowing polyvinyl alcohol film with high barrier, flame-retardant, and antibacterial effects. *Int. J. Biol. Macromol.* **2024**, *259*, 129240.

36 Wu, Y.; Tang, Q.; Yang, F.; Xu, L.; Wang, X.; Zhang, J. Mechanical and thermal properties of rice straw cellulose nanofibrils-enhanced polyvinyl alcohol films using freezing-and-thawing cycle method. *Cellulose* **2019**, *26*, 3193–3204.

37 Xia, Y.; Qian, S.; Zhang, X.; Zhang, Z.; Zhu, C. Biochar as an efficient reinforcing agent for poly(lactic acid)/poly(ε-caprolactone) biodegradable composites with high robustness and thermo-resistance. *Ind. Crop. Prod.* **2024**, *219*, 119049.

38 Wu, K.; Ye, Z.; Cheng, J.; Zeng, Y.; Wang, R.; Sun, W.; Kuang, Y.; Jiang, F.; Chen, S.; Zhao, X. Excellent thermal insulation and flame retardancy property of konjac glucomannan/sodium alginate aerogel reinforced by phytic acid. *Ind. Crop. Prod.* **2023**, *205*, 117495.

39 Zhang, Z.; Li, X.; Ma, Z.; Ning, H.; Zhang, D. Wang Y. A facile and green strategy to simultaneously enhance the flame retardant and mechanical properties of poly(vinyl alcohol) by introduction of a bio-based polyelectrolyte complex formed by chitosan and phytic acid. *Dalton Trans.* **2020**, *49*, 11226–11237.

40 Xu, Y.; Zhang, W.; Qiu, Y.; Xu, M.; Li, B.; Liu, L. Preparation and mechanism study of a high efficiency bio-based flame retardant for simultaneously enhancing flame retardancy, toughness and crystallization rate of poly(lactic acid). *Compos. Part B-Eng.* **2022**, *238*, 109913.

41 Lazar, S. T.; Kolibaba, T. J.; Grunlan, J. C. Flame-retardant surface treatments. *Nat. Rev. Mater.* **2020**, *5*, 259–75.

42 Xiong, Z.; Zhang, Y.; Du, X.; Song, P.; Fang, Z. Green and scalable fabrication of core-shell biobased flame retardants for reducing flammability of polylactic acid. *ACS Sustain. Chem. Eng.* **2019**, *7*, 8954–8963.

43 Chen, J.; Liu, Z.; Qiu, S.; Li, Y.; Sun, J.; Li, H.; Gu, X.; Zhang, S. A new strategy for the preparation of polylactic acid composites with flame retardancy, UV resistance, degradation, and recycling performance. *Chem. Eng. J.* **2023**, *472*, 145000.

44 Cheng, X.; Shi, L.; Fan, Z.; Yu, Y.; Liu, R. Bio-based coating of phytic acid, chitosan, and biochar for flame-retardant cotton fabrics. *Polym. Degrad. Stabil.* **2022**, *199*, 109898.

45 Li, Y.; Qiu, S.; Sun, J.; Ren, Y.; Wang, S.; Wang, X.; Wang, W.; Li, H.; Fei, B.; Gu, X.; Zhang, S. A new strategy to prepare fully bio-based poly(lactic acid) composite with high flame retardancy, UV resistance, and rapid degradation in soil. *Chem. Eng. J.* **2022**, *428*, 131979.

46 Jin, X.; Cui, S.; Sun, S.; Gu, X.; Li, X.; Liu, X.; Tang, W.; Sun, J.; Bourbigot, S, B.; Zhang, S. The preparation of a bio-polyelectrolytes based core-shell structure and its application in flame retardant polylactic acid composites. *Compos. Part A-Appl. Sci. Manuf.* **2019**, *124*, 105485.

47 Tian, J.; Kong, Y.; Qian, S.; Zhang, Z.; Xia, Y.; Li, Z. Mechanically robust multifunctional starch films reinforced by surface-tailored nanofibrillated cellulose. *Compos. Part B-Eng.* **2024**, *275*, 111339.

48 Zhang, S.; Zhang, Y.; Li, B.; Zhang, P.; Kan, L.; Wang, G.; Wei, H.; Zhang, X.; Ma, N. One-step preparation of a highly stretchable, conductive, and transparent poly(vinyl alcohol)–phytic acid hydrogel for casual writing circuits. *ACS Appl. Mater. Interfaces* **2019**, *11*, 32441–32448.

49 Xia, Y.; Qian, S.; Lu, W.; Zhang, Z.; Cheng, H.; Sheng, K. A strategy to prepare high-robust and ultra-tough polylactic acid/polycaprolactone/talc composites with thermo-resistance. *Polym. Compo.* **2023**, *44*, 8750–8765.

50 Mao, J.; Zhang, K.; Chen, B. Linking hydrophobicity of biochar to the water repellency and water holding capacity of biochar-amended soil. *Environ. Pollut.* **2019**, *253*, 779–789.

51 Li, L.; Xu, X.; Wang, B.; Song, P.; Cao, Q.; Yang, Y.; Xu, Z.; Wang, H. Structure, chain dynamics and mechanical properties of poly(vinyl alcohol)/phytic acid composites. *Compos. Commun.* **2021**, *28*, 100970.

https://doi.org/10.1007/s10118-025-3365-z